Study of several double-beta-decaying nuclei using the renormalized proton-neutron quasiparticle random-phase approximation

J. Toivanen and J. Suhonen
Department of Physics, University of Jyväskylä, P.O. Box 35, FIN-40351, Jyväskylä, Finland
(Received 31 May 1996)

The renormalized proton-neutron quasiparticle random-phase approximation model (RQRPA) has been used to calculate double-β-decay matrix elements and associated transition half-lives for two-neutrino double β decay of parent nuclei ^{76}Ge, ^{78}Kr, ^{82}Se, ^{96}Zr, ^{106}Cd, and ^{130}Te to the ground state and excited one- and two-phonon states of their daughter nuclei. The results are compared to ordinary proton-neutron QRPA and experiments. In addition, the violation of the Ikeda sum rule in the RQRPA is examined and discussed. [S0556-2813(97)00305-1]

PACS number(s): 23.40.Hc, 23.40.Bw, 21.60.Jz, 27.50.+e, 27.60.+j

I. INTRODUCTION

The proton-neutron quasiparticle random-phase approximation (pn QRPA) has proved to be a very powerful model, considering its simplicity, to describe nuclear matrix elements in ordinary β decay and the more complex two-neutrino ($2\nu\beta\beta$) and neutrinoless ($0\nu\beta\beta$) double β decays [1]. Historically, the long-lived problem of too fast theoretical double-β-decay rates was solved using pn QRPA by the introduction of the particle-particle channel of the proton-neutron interaction in the RPA matrices [2], making it possible to produce arbitrarily small double Gamow-Teller matrix elements (DGT). This dependence of the DGT matrix elements on particle-particle interaction strength g_{pp} has since then been reproduced also in the shell-model calculations [3] and is believed to be universal property of double-β-decay matrix elements in which the 1^+ states of the intermediate odd-odd nucleus have explicitly been taken into account.

However, one of the shortcomings of the ordinary pn QRPA reveals itself with the increasing strength of the proton-neutron interaction governed by the g_{pp} parameter. Near a certain critical interaction strength (usually beyond $g_{pp}=1$) the backward-going RPA amplitudes Y_{pn} of the first excited 1^+ state become overrated, causing the calculated double-β-decay amplitudes to diverge. The reason for this overrating is an increasing violation of the Pauli exclusion principle, or in other words, lack of feedback of the ground-state correlations in the RPA equations. Therefore, ordinary RPA builds too strong ground-state correlations too early. Sometimes this overrating has started already for quite weak particle-particle interaction strengths (g_{pp} around 0.7–0.8) making it difficult to reliably extract double-β-decay information from the calculation.

Several attempts have been made in the past to shift the collapse of the pn QRPA to higher values of g_{pp} [4–7]. All these methods, however, disregard the main source of ground-state instability, namely, the increasing violation of the Pauli principle with a build up of excessive amounts of ground-state correlations. To overcome this difficulty we have proposed in [8] to use a self-consistent iteration of the renormalized pn QRPA equations to take into account the one-body densities of the correlated QRPA ground state in evaluating the A and B matrices of the RPA equations. This scheme of calculation we call the renormalized proton-neutron QRPA, i.e., the RQRPA.

In this article we use the RQRPA in connection with the multiple-commutator method (MCM) of [9] to study double β^- decays of nuclei ^{76}Ge, ^{82}Se, ^{96}Zr, and ^{130}Te and double β^+/EC decays of nuclei ^{78}Kr and ^{106}Cd to the ground state and excited one- and two-phonon states of their daughter nuclei. We also study how much the RQRPA violates, in a realistic calculation, the Ikeda sum rule which is conserved in the ordinary pn QRPA.

Our article is ordered as follows: in Sec. II the necessary theoretical framework is reviewed and then applied in Sec. III, where the results are presented and analyzed. Finally, in Sec. IV, the conclusions are drawn.

II. FORMALISM

In the renormalized pn QRPA treatment the creation and annihilation operators of excited states are restricted to have only two-quasiparticle components and have the same structure as in the ordinary pn QRPA:

$$Q^\dagger(m;JM)=\sum_{pn}\left[X_{pn}^{Jm}A^\dagger(pn;JM)-Y_{pn}^{Jm}\tilde{A}(pn;JM)\right]. \tag{1}$$

The equations-of-motion method (EOM) of [10] produces an RPA-like system of equations for the forward- and backward-going amplitudes X_{pn}^{Jm} and Y_{pn}^{Jm}:

$$\begin{pmatrix} A & B \\ B & A \end{pmatrix}\begin{pmatrix} X^{Jm} \\ Y^{Jm} \end{pmatrix}=\omega_{Jm}\begin{pmatrix} U & 0 \\ 0 & -U \end{pmatrix}\begin{pmatrix} X^{Jm} \\ Y^{Jm} \end{pmatrix}. \tag{2}$$

The matrices A and B are derived from the commutator equations

$$A(pnp'n'J)=\langle \text{g.s.}|[A(pn;JM),\hat{H},A^\dagger(p'n';JM)]|\text{g.s.}\rangle, \tag{3a}$$

$$B(pnp'n'J)=\langle \text{g.s.}|[A(pn;JM),\hat{H},A(p'n';JM)]|\text{g.s.}\rangle, \tag{3b}$$

where $2[A,B,C]=[A,[B,C]]+[[A,B],C]$ and $\hat{H}$ is the nuclear Hamiltonian. Here the expectation value has been taken in the correlated pn QRPA ground state $|\text{g.s.}\rangle$, which is substituted by the BCS ground state on the level of the ordinary pn QRPA.

The commutators in Eq. (3) have, in addition to ordinary *scalar* RPA terms, additional terms proportional to $a^\dagger a$ and $a^\dagger a^\dagger aa$, in other words, terms depending on one- and two-quasiparticle densities. These terms take into account the Pauli exclusion principle. In order to keep the model tractable we have made the following approximations. First of all, the two-quasiparticle densities in Eq. (3) have not been included because of their complexity, see the discussion in Ref. [10]. This is our biggest approximation and assumes a random-phase cancellation of these terms.

On the right-hand side of Eq. (2) we have written matrix U, the overlap matrix between the two-quasiparticle states. It consists of one-quasiparticle densities of the form

$$\begin{aligned} U(pnp'n') &= \langle \text{g.s.}|[A(pn;JM),A^\dagger(p'n';JM)]|\text{g.s.}\rangle \\ &= \delta_{pp'}\delta_{nn'} - \delta_{nn'}\hat{j}_p^{-1}\langle \text{g.s.}|[a_p^\dagger \tilde{a}_{p'}]_{00}|\text{g.s.}\rangle \\ &\quad - \delta_{pp'}\hat{j}_n^{-1}\langle \text{g.s.}|[a_n^\dagger \tilde{a}_{n'}]_{00}|\text{g.s.}\rangle, \end{aligned} \tag{4}$$

and can be approximated diagonal, i.e.,

$$\begin{aligned} U(pnp'n') &= \delta_{pp'}\delta_{nn'}(1-\hat{j}_p^{-1}\langle \text{g.s.}|[a_p^\dagger \tilde{a}_p]_{00}|\text{g.s.}\rangle \\ &\quad -\hat{j}_n^{-1}\langle \text{g.s.}|[a_n^\dagger \tilde{a}_n]_{00}|\text{g.s.}), \\ &= \delta_{pp'}\delta_{nn'}(1-q_p-q_n) = \delta_{pp'}\delta_{nn'}U_{pn}, \end{aligned} \tag{5}$$

where $\hat{j}=\sqrt{2j+1}$. This is not a bad approximation at all, because if the single-particle basis has at most two oscillator major shells, the off-diagonal matrix elements vanish altogether because of spin and parity conservation. A diagonal norm matrix makes it possible to transform Eq. (2) into an ordinary RPA-type of equation:

$$\begin{pmatrix} \overline{A} & \overline{B} \\ \overline{B} & \overline{A} \end{pmatrix} \begin{pmatrix} \overline{X^{Jm}} \\ \overline{Y^{Jm}} \end{pmatrix} = \omega_{Jm} \begin{pmatrix} \overline{X^{Jm}} \\ -\overline{Y^{Jm}} \end{pmatrix}, \tag{6}$$

where, now the RPA A and B matrices are renormalized by the factors U_{pn}:

$$\begin{aligned} \overline{A}(pnp'n'J) &= (E_p+E_n)\delta_{pp'}\delta_{nn'} - U_{pn}^{1/2}[2G(pnp'n'J) \\ &\quad \times(u_p u_n u_{p'} u_{n'} + v_p v_n v_{p'} v_{n'}) \\ &\quad + 2F(pnp'n'J)(u_p v_n u_{p'} v_{n'} \\ &\quad + v_p u_n v_{p'} u_{n'})]U_{p'n'}^{1/2}, \end{aligned} \tag{7a}$$

$$\begin{aligned} \overline{B}(pnp'n'J) &= U_{pn}^{1/2}[2G(pnp'n'J)(u_p u_n v_{p'} v_{n'} \\ &\quad + v_p v_n u_{p'} u_{n'}) - 2F(pnp'n'J)(u_p v_n v_{p'} u_{n'} \\ &\quad + v_p u_n u_{p'} v_{n'})]U_{p'n'}^{1/2}, \end{aligned} \tag{7b}$$

$$\overline{X_{pn}^{Jm}} = U_{pn}^{1/2} X_{pn}^{Jm}, \quad \overline{Y_{pn}^{Jm}} = U_{pn}^{1/2} Y_{pn}^{Jm}.$$

Amplitudes (7b) fulfill the usual RPA orthonormality relations. The quasiparticle occupation numbers used in matrices A, B, and U can easily be evaluated [11-13] and are given by

$$q_p = \hat{j}_p^{-2}\sum_n \left(\sum_{Jm} \hat{J}^2 |\overline{Y_{pn}^{Jm}}|^2 \right)(1-q_p-q_n), \tag{8a}$$

$$q_n = \hat{j}_n^{-2}\sum_p \left(\sum_{Jm} \hat{J}^2 |\overline{Y_{pn}^{Jm}}|^2 \right)(1-q_p-q_n). \tag{8b}$$

As discussed in Refs. [14–16] this form of quasiparticle occupation numbers is slightly erroneous because it overcounts the ground-state correlations. However, the overcounting causes very little error in practical calculations. In the RQRPA the Eqs. (6) and (8) must be fulfilled simutaneously, making the diagonalization problem nonlinear and subject to iterative solution [8].

The double-β-decay matrix elements have the general form [17]

$$M_{\text{DGT}} = \sum_m \frac{\beta_m^+ \beta_m^-}{\{[(1/2)Q_{\beta\beta}+E_m-M_i]/m_e+1\}^s}, \tag{9}$$

where $Q_{\beta\beta}$ is the double-β-decay Q value, M_i is the mass energy of the initial nucleus, $s=1$ for $J=0$, and $s=3$ for $J=2$. The quantity E_m is the (total) energy of the mth intermediate 1^+ state, i.e., the relative spacing of the energies E_m is coming from the roots ω_{1m} of Eq. (6). The difference E_1-M_i in Eq. (9) is taken from the known nuclear masses (nuclear mass difference of the intermediate and initial nucleus) and the experimental excitation energy of the first 1^+ state with respect to the ground state of the intermediate nucleus. After this phenomenological scaling of the first (R)QRPA root the difference E_m-E_1 has been taken as average of the corresponding differences $\omega_{1m}-\omega_{11}$ for the initial and final (R)QRPA calculations discussed below. The quantity $Q_{\beta\beta}$ was taken from the experimental data.

The matrix elements $\beta_m^\pm$ of the β-decay operators are written as [17]

$$\beta_m^- = (1_m^+ \| \hat{\beta}^- \| 0_i^+), \tag{10}$$

$$\beta_m^+ = \sum_{m'} (J_f^+ \| \hat{\beta}^- \| 1_{m'}^+) \langle 1_{m'}^+ | 1_m^+ \rangle. \tag{11}$$

In the RQRPA the β-decay amplitudes (10) and (11) are modified (see [8]) by the introduction of factors $U_{pn}^{1/2}$ multiplying the amplitudes $\overline{X_{pn}^{Jm}}$ and $\overline{Y_{pn}^{Jm}}$ in the formulas of [17].

Two separate QRPA calculations, both either of the pn QRPA or of the RQRPA type, have to be done in evaluating the DGT matrix element of Eq. (9), namely one for the initial [the amplitude of Eq. (10)] and the other for the final nucleus [the amplitude of Eq. (11)]. These calculations are based on (slightly) different single-particle energies and thence on different BCS vacua so that the u and v factors appearing in Eqs. (7) are different for the initial and final nuclei. The eigenvalue problem of Eq. (6) is then solved separately for the initial and final nucleus leading to self-consistent iteration of the quantities $\overline{X_{pn}^{1m}}$, $\overline{Y_{pn}^{1m}}$, ω_{1m}, and $U_{pn}^{1/2}$ for these

TABLE I. The WS and AWS proton and neutron single-particle energies near the Fermi surface for ^{76}Ge and ^{76}Se. Only orbitals having BCS quasiparticle energies below 5 MeV are listed.

^{76}Ge					
	Protons			Neutrons	
	WS	AWS		WS	AWS
$1p_{1/2}$	−6.79	−6.79	$1p_{1/2}$	−9.80	−8.50
$1p_{3/2}$	−9.01	−9.01	$1p_{3/2}$	−11.5	−9.50
$0f_{5/2}$	−8.21	−8.70	$0f_{5/2}$	−10.7	−10.7
$0g_{9/2}$	−5.31	−8.00	$0g_{9/2}$	−7.03	−9.00
^{76}Se					
	Protons			Neutrons	
	WS	AWS		WS	AWS
$1p_{1/2}$	−5.00	−6.00	$1p_{1/2}$	−11.0	−9.50
$1p_{3/2}$	−7.00	−7.00	$1p_{3/2}$	−12.8	−10.4
$0f_{5/2}$	−6.29	−6.10	$0f_{5/2}$	−12.0	−10.3
$0g_{9/2}$	−3.37	−5.60	$0g_{9/2}$	−8.30	−10.0
			$1d_{5/2}$	−4.30	−4.30

nuclei. The two emerging sets of intermediate 1^+ states are projected upon each other by introducing the overlap $\langle 1^+_{m'}|1^+_m\rangle$ of Eq. (11) containing the two sets of u, v, X, and Y amplitudes as given in [17].

III. RESULTS AND DISCUSSION

Two sets of single-particle energies were used in the calculations. The first set consisted of Coulomb-corrected Woods-Saxon (WS) energies with Bohr-Mottelson parametrization. The second set (AWS) consisted of WS energies adjusted near the Fermi level to yield better agreement between the BCS-calculated one-quasiparticle spectra and experimental energies of corresponding odd-proton and odd-neutron nuclei. This adjusted basis is the one of Ref. [18] and both the WS and the AWS single-particle energies for the $A=78$, $A=106$, and $A=130$ nuclei are shown in that article. For the rest of the nuclei, discussed in the present article, the WS and AWS single-particle energies are shown in Tables I ($A=76$), II ($A=82$), and III ($A=96$). The residual interaction was obtained from G matrix derived from the Bonn-A potential. Two oscillator major shells, plus intruder orbitals from the next higher oscillator major shell, were used for both protons and neutrons as the valence space of each studied nucleus.

The calculational procedure, except for the solution of the RQRPA equations, was the same as in Ref. [18]. Each double-β calculation contains two RQRPA or pn QRPA calculations, namely, one for the initial and the other for the final nucleus. The pairing part of the calculation contains four adjustable parameters: one for the proton and one for the neutron pairing interaction separately adjusted in the initial and final BCS calculation. Two more parameters are needed for the 1^+ channel of the proton-neutron interaction, namely, one for the particle-hole and the other for the particle-particle part of it (these parameters are taken to be the same in the initial and final calculations). The pairing parameters are adjusted to odd-even mass differences and the particle-hole parameter g_{ph} of the proton-neutron 1^+ interaction to the semiempirical location of the Gamow-Teller giant resonance (GTGR). We have used the ordinary pp-nn QRPA [19] to calculate the 2^+_1 and two-phonon states of the double-β daughter nuclei, and the RQRPA for intermediate 1^+ states in Eq. (9). The particle-hole part of the like-particle quadrupole interaction is scaled to reproduce the experimental energy of the 2^+_1 state in the daughter nuclei. Otherwise the two-body matrix elements of the quadrupole channel retain their G-matrix values.

TABLE II. The WS and AWS proton and neutron single-particle energies near the Fermi surface for ^{82}Se and ^{82}Kr. Only orbitals having BCS quasiparticle energies below 5 MeV are listed.

^{82}Se					
	Protons			Neutrons	
	WS	AWS		WS	AWS
$1p_{1/2}$	−8.14	−8.14	$1p_{1/2}$	−10.7	−8.99
$1p_{3/2}$	−10.1	−10.0	$0f_{5/2}$	−11.8	−11.8
$0f_{5/2}$	−9.69	−11.5	$2s_{1/2}$	−2.83	−2.83
$0f_{7/2}$	−15.1	−15.1	$1d_{5/2}$	−4.12	−4.12
$0g_{9/2}$	−6.67	−6.67	$0g_{9/2}$	−8.01	−8.01
^{82}Kr					
	Protons			Neutrons	
	WS	AWS		WS	AWS
$1p_{1/2}$	−6.29	−6.59	$1p_{1/2}$	−11.8	−9.99
$1p_{3/2}$	−8.31	−8.39	$1p_{3/2}$	−13.5	−13.5
$0f_{5/2}$	−7.84	−7.59	$0f_{5/2}$	−13.0	−13.0
$0f_{7/2}$	−13.2	−13.2	$1d_{5/2}$	−5.09	−5.09
$0g_{9/2}$	−4.86	−6.29	$0g_{9/2}$	−9.21	−9.21

TABLE III. The WS and AWS proton and neutron single-particle energies near the Fermi surface for ^{96}Zr. Only orbitals having BCS quasiparticle energies below 5 MeV are listed. For ^{96}Mo the AWS basis coincides with the WS one and only the WS energies are given.

^{96}Zr					
	Protons			Neutrons	
	WS	AWS		WS	AWS
$1p_{1/2}$	−9.14	−9.20	$2s_{1/2}$	−4.90	−5.60
$1p_{3/2}$	−11.2	−11.2	$1d_{3/2}$	−4.04	−4.04
$0f_{5/2}$	−11.4	−11.4	$1d_{5/2}$	−6.53	−6.53
$0g_{9/2}$	−8.19	−9.00	$0g_{7/2}$	−4.91	−4.91
			$0g_{9/2}$	−10.7	−10.7
			$0h_{11/2}$	−2.57	−2.57
^{96}Mo					
	Protons			Neutrons	
$1p_{1/2}$		−7.71	$2s_{1/2}$		−5.70
$1p_{3/2}$		−9.51	$1d_{3/2}$		−4.84
$0f_{5/2}$		−9.69	$1d_{5/2}$		−7.44
$0g_{9/2}$		−6.53	$0g_{7/2}$		−5.85
			$0g_{9/2}$		−11.8
			$0h_{11/2}$		−3.55

It is worth noting that usually the 2_1^+ state turns out to be rather collective both experimentally and in the pp-nn QRPA, stressing the importance of quadrupole vibrations in spherical and nearly spherical nuclei. The collectivity manifests itself, for example, in the rather large value of the $B(E2;2_1^+ \rightarrow 0_{\text{g.s.}}^+)$. This is a feature which the present formalism can qualitatively, and even quantitatively (see, e.g., Table II of Ref. [17]), reproduce by the collective 2_1^+ pp-nn QRPA phonon. On the other hand, it is well known [20] that the RPA has difficulties in predicting static quadrupole moments of some one-phonon quadrupole excitations, like in the case of ^{76}Se. This is clearly a deficiency of our approach. Another shortcoming is that the data on the crossover transition rate $B(E2;2_2^+ \rightarrow 0_{\text{g.s.}}^+)$ cannot be reproduced due to the simple two-phonon structure of the theoretical 2_2^+ state leading to zero value for the theoretical crossover transition rate. This deficiency has also been seen in double-β-decay calculations, namely in the case of ^{100}Mo decay [21] and in previous treatments of ^{130}Te [18]. It is present also in our calculations and we will discuss it more extensively in connection with the ^{130}Te decay below.

To improve the theoretical description in this respect, one should go beyond the simple multiphonon picture and take into account the interaction of the two-phonon states with their surroundings, e.g., by using the boson-expansion techniques [22]. Such improvements of the present MCM formalism could lead to considerable changes in the theoretical $2\nu\beta\beta$ decay rates to the 0_2^+ and 2_2^+ states, and should be studied in the future.

In the self-consistent iteration of the RQRPA all the intermediate multipolarities appear in the evaluation of the quasiparticle occupations of Eqs. (8). Numerical calculations show that only a limited set of these multipolarities play a role in the evaluation of these occupations. In the present calculations the multipolarities 1^+, 1^-, 2^-, 3^+, and 4^- are enough to guarantee accurate evaluation of q_p and q_n in Eqs. (8).

In the present article we use a simple method to set the value of g_{pp} for each nucleus. For the cases where experimental information about the $2\nu\beta\beta$ ground-state transition is available we use it to fix the value of g_{pp} and use this value to calculate theoretical half-lives for transitions to other final states (i.e., 0_2^+, 2_1^+, and 2_2^+ states). When there is no such information, as in the case of ^{78}Kr and ^{106}Cd, we have calculated all transition half-lives with $g_{pp}=1.0$.

Table IV summarizes the RQRPA, and Table V the pn QRPA results for transition half-lives of the nuclei under discussion. The ground-state transition and the transitions to $0_2^+, 2_1^+$, and 2_2^+ states have been included and the corresponding half-lives compared with the data. For the RQRPA results we have used the above-mentioned method of setting the value of g_{pp} but for the pn QRPA this is not possible in the cases where the value $g_{pp}=1.0$ is very close or beyond the collapse of the pn QRPA. This leaves only four nuclei in Table V for which theoretical half-life values can be given within the pn QRPA description. For the other cases one would need additional information, e.g., data on single β-decay transitions, see Ref. [18], to set the value of g_{pp}.

To illustrate the differences between the pn QRPA and the RQRPA and to show the stability of the RQRPA solution, we plot in Figs. 1–5 the calculated DGT matrix element M_{DGT} as a function of g_{pp} for the RQRPA and the pn QRPA. In Figs. 1(a) and 1(b) we show the effect of different single-particle energies by displaying the pn QRPA and RQRPA results separately for the two basis sets (WS and AWS).

In ^{76}Ge [Fig. 1(b)] and in ^{130}Te (Fig. 3) the pn QRPA collapses very early in the AWS single-particle basis. This is due to the strong ground-state correlations caused by the increased level density near the proton and neutron fermi surfaces in the adjusted single-particle basis. For ^{76}Ge the RQRPA is able to push the zero-crossing point of M_{DGT} from 0.75 to 1.1. Furthermore, the RQRPA reproduces the experimental double-β half-life of ^{76}Ge for the ground-state transition when g_{pp} acquires the values 1.04 (WS) and 1.07 (AWS). By using these values of g_{pp} the two basis sets give almost identical half-lives for transitions to the other final

TABLE IV. Double-β-decay half-lives for transitions to different final states calculated using the RQRPA.

			^{76}Ge		
	g_{pp}	g.s.	0_2^+	2_1^+	2_2^+
WS	1.04	1.4×10^{21}	1.0×10^{23}	1.0×10^{26}	2.2×10^{28}
AWS	1.07	1.4×10^{21}	3.1×10^{23}	1.0×10^{26}	7.2×10^{27}
exp.		1.4×10^{21}	$>4.1\times10^{21}$	$>3.0\times10^{21}$	$>3.3\times10^{21}$
			^{82}Se		
	g_{pp}	g.s.	0_2^+	2_1^+	2_2^+
WS	1.02	1.1×10^{20}	3.3×10^{21}	2.8×10^{23}	3.0×10^{23}
AWS	1.11	1.1×10^{20}	1.6×10^{21}	1.5×10^{24}	1.5×10^{23}
exp.		1.1×10^{20}	$>1.2\times10^{21}$	$>6.6\times10^{20}$	
			^{96}Zr		
	g_{pp}	g.s.	0_2^+	2_1^+	2_2^+
WS	1.20	4.2×10^{19}	2.4×10^{21}	3.8×10^{21}	6.3×10^{24}
AWS	1.29	4.4×10^{19}	2.7×10^{21}	4.8×10^{21}	6.0×10^{24}
exp.		3.9×10^{19}	$>3.3\times10^{19}$	$>4.1\times10^{19}$	
			^{130}Te		
	g_{pp}	g.s.	0_2^+	2_1^+	2_2^+
WS	0.79	2.7×10^{21}	2.6×10^{20}	1.4×10^{23}	3.2×10^{26}
AWS	0.72	2.7×10^{21}	7.1×10^{20}	3.0×10^{22}	2.0×10^{25}
exp.		2.7×10^{21} [a]		$>4.5\times10^{21}$	
			^{78}Kr		
	g_{pp}	g.s.	0_2^+		
WS	1.0	6.8×10^{22}	2.1×10^{27}		
AWS	1.0	8.2×10^{21}	4.7×10^{24}		
exp.		$>1.1\times10^{20}$			
			^{106}Cd		
	g_{pp}	g.s.	0_2^+		
WS	1.0	2.1×10^{20}	1.0×10^{22}		
AWS	1.0	2.0×10^{20}	1.4×10^{23}		
exp.		$>2.6\times10^{17}$			

[a]The experimental value is geochemical one containing all final states, see discussion in text.

TABLE V. Double-β-decay half-lifes for transitions to different final states calculated using the pn QRPA.

			^{76}Ge		
	g_{pp}	g.s.	0_2^+	2_1^+	2_2^+
WS	0.80	1.4×10^{21}	1.1×10^{23}	8.6×10^{25}	2.5×10^{28}
AWS	0.77	1.4×10^{21}	2.1×10^{22}	4.0×10^{24}	3.0×10^{29}
exp.		1.4×10^{21}	$>4.1\times10^{21}$	$>3.0\times10^{21}$	$>3.3\times10^{21}$
			^{82}Se		
	g_{pp}	g.s.	0_2^+	2_1^+	2_2^+
WS	0.96	1.1×10^{20}	2.8×10^{21}	2.4×10^{23}	2.8×10^{24}
AWS	0.96	1.1×10^{20}	1.3×10^{21}	5.8×10^{23}	1.3×10^{24}
exp.		1.1×10^{20}	$>1.2\times10^{21}$	$>6.6\times10^{20}$	
			^{96}Zr		
	g_{pp}	g.s.	0_2^+	2_1^+	2_2^+
WS	0.94	1.5×10^{18}	2.3×10^{21}	2.8×10^{21}	1.4×10^{25}
AWS	1.09	3.9×10^{19}	2.3×10^{21}	3.0×10^{21}	1.3×10^{25}
exp.		3.9×10^{19}	$>3.3\times10^{19}$	$>4.1\times10^{19}$	
			^{130}Te		
	g_{pp}	g.s.	0_2^+	2_1^+	2_2^+
WS	0.74	2.7×10^{21}	2.4×10^{20}	1.3×10^{23}	2.8×10^{26}
AWS	0.64	2.7×10^{21}	6.2×10^{20}	2.5×10^{22}	1.3×10^{26}
exp.		2.7×10^{21} [a]		$>4.5\times10^{21}$	

[a]The experimental value is geochemical one containing all final states, see discussion in text.

states, as can be seen from Table IV. The only exception is the 2_2^+ transition. This is due to the interesting fact that in the AWS basis the pn QRPA and the RQRPA deviate from each other already for small g_{pp}. At this point it is appropriate to comment that the inclusion of the $0h_{9/2}$ orbital in the present calculation affects somewhat the double-β matrix elements as seen by comparing the present result for the WS basis [Fig. 1(a)] with the corresponding one of Fig. 7(a) of Ref. [17] where the $0h_{9/2}$ orbital was omitted. In Ref. [18] the contribution of this orbital to some single-β-decay transitions was found to be rather important and that is why it is included also in the present calculation.

The difference in results between the two basis sets is largest in the case of ^{130}Te. For the WS basis the pn QRPA and the RQRPA amplitudes differ only very little around $g_{pp}=1.0$, indicating that in this basis both the pn QRPA and the RQRPA build relatively little ground-state correlations on top of the BCS vacuum. In the AWS basis (Fig. 3) the pn QRPA collapses already at $g_{pp}=0.79$ and the RQRPA is not able to push the zero-crossing point of M_{DGT} to substantially higher g_{pp} values.

At this point it is important to note that the experimental half-life value for ^{130}Te in Tables IV and V is based on geochemical measurements and contains transition amplitudes to all possible final states. Due to the difficulties with the description of the 0_2^+ final state as a two-phonon state, as mentioned earlier, both pn QRPA and RQRPA produce too large matrix elements for the transition to the 0_2^+ state in ^{130}Te, and it is impossible to fit the total theoretical half-life to the experimental half-life. In this case the simple two-

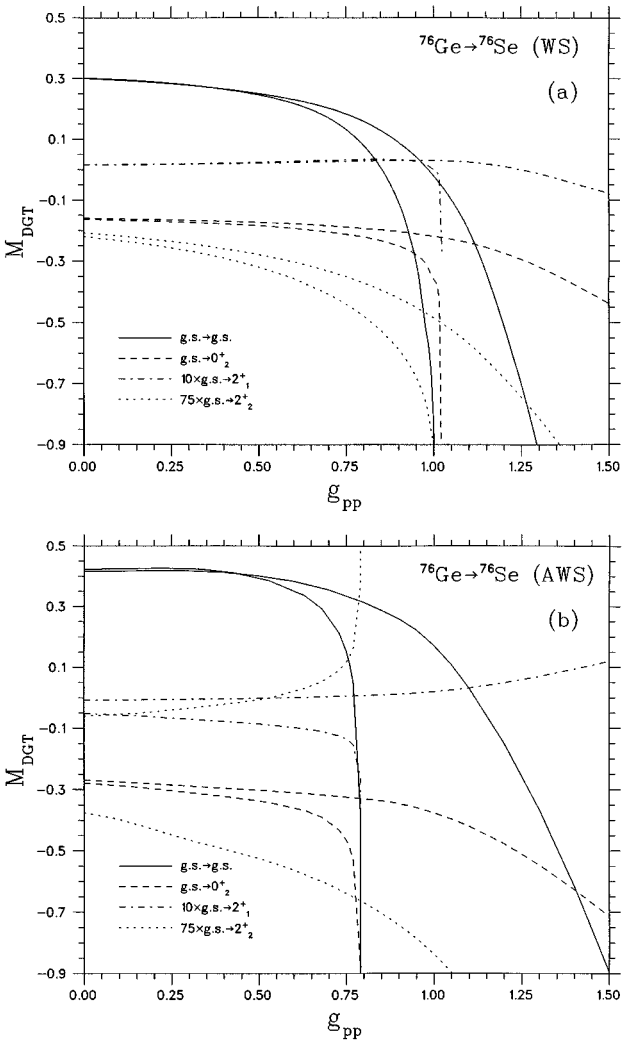

FIG. 1. The DGT matrix element as a function of g_{pp} for ^{76}Ge in the WS single-particle basis (a) and in the AWS single-particle basis (b). The curves extending to higher g_{pp} values, for each line type, are obtained by the RQRPA, and the curves with a more sudden change in the magnitude of the DGT near the critical g_{pp} are obtained by using the pn QRPA.

phonon picture for the 0_2^+ state is clearly inadequate. Assuming that the true decay rate to the 0_2^+ state is negligible in comparison with the ground-state one, we have fitted the theoretical ground-state transition rate to the experimental value. In both basis sets the experimental half-life value is reproduced by a rather low value of g_{pp}, as seen in Tables IV and V. These tables also indicate that the predicted half-lives for the excited-state transitions are very similar in the pn QRPA and the RQRPA, except for the 2_2^+ transition in the AWS basis.

For the parent nuclei ^{82}Se and ^{96}Zr the WS and the AWS basis sets give very similar transition half-lives for the excited states. The only exception is the 2_1^+ transition in ^{82}Se in the RQRPA formalism, as seen in Table V. As an example, we show in Fig. 2 the decay of ^{96}Zr in the AWS basis. As mentioned in the caption of Table III, the AWS and the WS single-particle energies are identical in the daughter nucleus ^{96}Mo (the WS basis already gives correct quasiparticle energies). Here the RQRPA corrections to transition

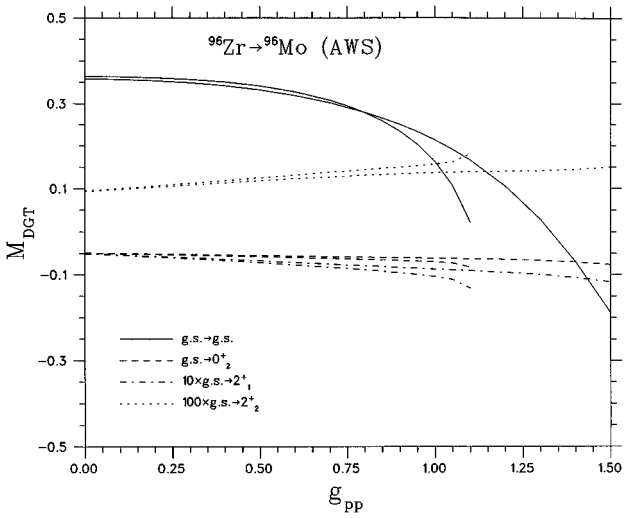

FIG. 2. The DGT matrix element as a function of g_{pp} for ^{96}Zr in the AWS single-particle basis. The *pn* QRPA and the RQRPA results can be identified as explained in the caption of Fig. 1.

half-lives are practically negligible up to the collapse of the *pn* QRPA. The adopted g_{pp} values for the RQRPA and the *pn* QRPA are shown in Tables IV and V. For these values the RQRPA and the *pn* QRPA reproduce the ground-state transition half-life. However, there is one exception: the *pn* QRPA in the WS basis. In this case one cannot reproduce the experimental half-life by any value of g_{pp} (see Ref. [18] for details) and in Table V we only list the g_{pp} value which produces the minimum value for the ground-state DGT matrix element.

Figure 4 shows the DGT transition amplitudes for the double β^+/EC decaying nucleus ^{78}Kr. The g_{pp} values for all transitions are set to 1.0 in the RQRPA. As in the case of ^{76}Ge, the *pn* QRPA collapses too early for the AWS basis, but the RQRPA prevents the DGT matrix element from crossing zero too early. In the WS basis the ground-state

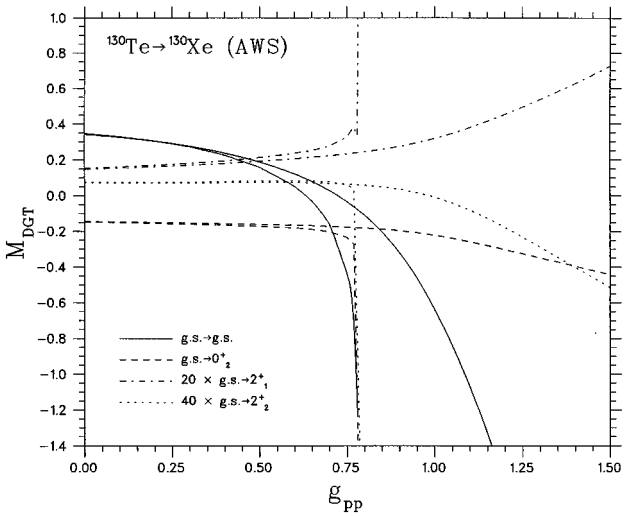

FIG. 3. The DGT matrix element as a function of g_{pp} for ^{130}Te in the AWS single-particle basis. The *pn* QRPA and the RQRPA results can be identified as explained in the caption of Fig. 1.

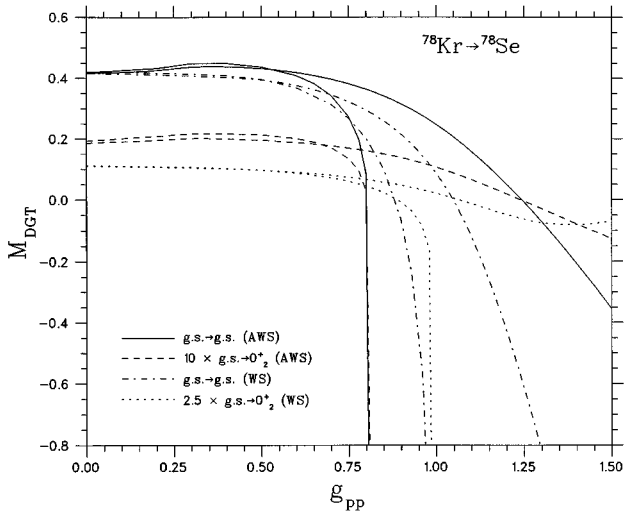

FIG. 4. The DGT matrix elements of ^{78}Kr in the WS and AWS bases for decays to the 0^+ final states as functions of g_{pp}. The *pn* QRPA and the RQRPA results can be identified as explained in the caption of Fig. 1.

correlations are weaker as also the RQRPA corrections to M_{DGT}.

Figure 5 displays the DGT transition amplitudes for the β^+/EC decaying nucleus ^{106}Cd. The g_{pp} value for all transitions is set to 1.0 in the RQRPA. Around $g_{pp}=1.0$ both basis sets give similar ground-state half-lives in the RQRPA, whereas the half-lives for the excited-state transitions differ to some extent from each other.

As a general conclusion of the above analysis it can be said that the predictive power of the QRPA formalism, based on proton-neutron quasiparticle pairs, is poor if there is no experimental information on the $2\nu\beta\beta$-decay rate to the ground state available. Alternatively, a study of the lateral β-decay feeding has to be done in order to estimate the appropprate value of g_{pp} [18]. Use of either of the aforementioned data in connection with the QRPA framework yields definite theoretical predictions for the $2\nu\beta\beta$ decay rates to

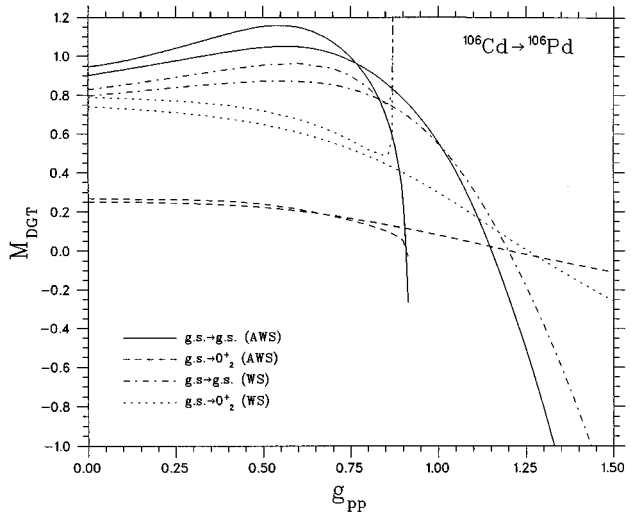

FIG. 5. The same as Fig. 4 for the decay of ^{106}Cd.

excited states. It has to be noted that in the RQRPA one always can make a first estimate of the $2\nu\beta\beta$-decay rates by taking $g_{pp}=1.0$. The quality of the resulting decay-rate estimates depends on the stability of the theoretical decay amplitudes in the neighborhood of $g_{pp}=1.0$. As seen in Figs. 1–5, in many cases the stability of the excited-state transitions is far better than the stability of the ground-state transition so that more unique theoretical estimates for the decay rates to the excited states can be expected. In the pn QRPA even this very naive estimation is not always possible because sometimes the pn QRPA breaks down before the value $g_{pp}=1.0$.

Finally, we want to discuss the conservation of the Ikeda sum rule $S_I \equiv S_- - S_+ = 3(N-Z)$ in the RQRPA framework. Here S_- (S_+) is the total summed Gamow-Teller β^- (β^+) transition strength from the ground state of an even-even nucleus. In the pn QRPA the Ikeda sum rule is exactly conserved if all the spin-orbit partners of the single-particle orbitals in the chosen valence space are included. Even omitting some of these partners, in practice those lying a magic shell gap apart from the valence space, does not lead to essential violation of the sum rule.

In the RQRPA the sum rule is violated even if all the spin-orbit partners are included in the single-particle basis. This violation is to be attributed to the incompleteness of the RQRPA phonon (1), i.e., to omission of the scattering terms [23] in the definition of the phonon. Restoration of the average neutron and proton numbers in the RQRPA has a very small effect upon the Ikeda sum rule. This can be seen from the average particle numbers of the RQRPA ground state which deviate from the BCS values by only a few percent. The main correction thus comes from the scattering terms and their role can be seen from the following form of the sum rule:

$$S_- - S_+ = \sum_\mu (-1)^\mu \langle 0|[\hat{\beta}^+_\mu, \hat{\beta}^-_{-\mu}]|0\rangle. \qquad (12)$$

In Eq. (12) the quasiparticle representation of the β-decay operators $\hat{\beta}^\pm_\mu$ contains also scattering contributions [17] which take part in the commutator of the right-hand side of Eq. (12). In the QRPA level of approximation the real ground state $|0\rangle$ is substituted by the BCS ground state and thus the scattering contribution vanishes leading to consistency in the evaluation of the left-hand and right-hand sides of Eq. (12). In the RQRPA level of approximation one uses the real ground state and thus nonzero scattering contributions are expected from the right-hand side of Eq. (12). This unbalances Eq. (12) since on the left-hand side one still evaluates the quantities S_- and S_+ by using the phonon (1) without any scattering terms.

The magnitude and nature of the violation has been studied in Figs. 6–8. There we plot the relative β^- strength $S_-/3(N-Z)$ [Fig. 6(a)] and the relative β^+ strength $S_+/3(N-Z)$ [Fig. 6(b)] as a function of g_{pp} in the pn QRPA approach for all the $2\nu\beta\beta$ mother nuclei under study. In Figs. 7(a) and 7(b) we do the same for the RQRPA approach. Finally, in Fig. 8 we combine the data of Figs. 6 and 7 and show the ratio of the RQRPA sum S_I(RQRPA) and the exact sum $S_I=3(N-Z)$ as a function of g_{pp}. For comparison we have added here also a curve for ^{100}Mo from our earlier

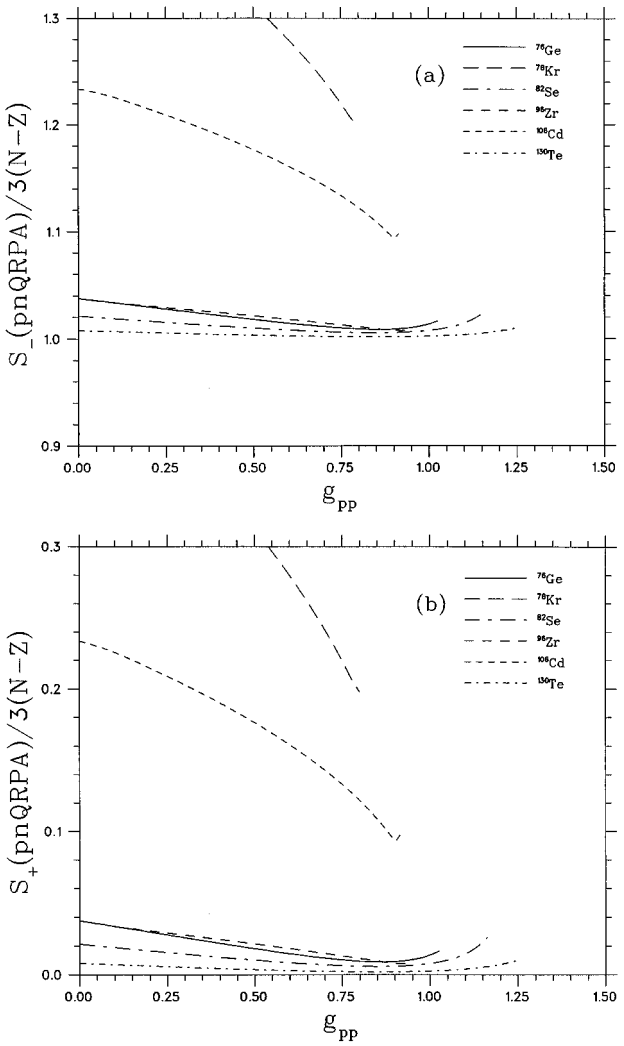

FIG. 6. The relative β^- strength (a) and β^+ strength (b) as a function of g_{pp} in the pn QRPA approach for different $2\nu\beta\beta$ mother nuclei. The curves extend up to the breaking point of the pn QRPA.

work [8]. The emerging pattern for the final nuclei exhibits the same features and thus the corresponding figures are not drawn for them. By comparing Figs. 6(a) and 7(a) one notices that S_-(RQRPA) is smaller than $S_-(pn\text{QRPA})$ for all values of g_{pp}. The difference between these two summed strengths increases with increasing g_{pp} leading to clear underestimation of S_- by the RQRPA when approaching the breakdown point of the pn QRPA. Comparing the summed β^+ strengths S_+(RQRPA) and $S_+(pn\text{QRPA})$ of Figs. 6(b) and 7(b), one observes that up to the break-down of the pn QRPA the RQRPA and the pn QRPA give the same result. This is true for all the other $2\nu\beta\beta$ mother nuclei except for ^{76}Ge for which the RQRPA overestimates S_+.

From Fig. 8 one sees that for the RQRPA the deviation from the exact Ikeda sum rule depends on the nuclear mass, being smaller for the heavier nuclei ($A\geqslant 96$) than for the lighter ones ($A\leqslant 82$). The magnitude of the violation is $3-20$ % at $g_{pp}=1.0$. Thus, at least for the heavier nuclei, the RQRPA model does not lose too much of the GT sum rule. The analysis of Figs. 6 and 7 reveals that the deviation can be associated solely to underestimation of the β^- branch

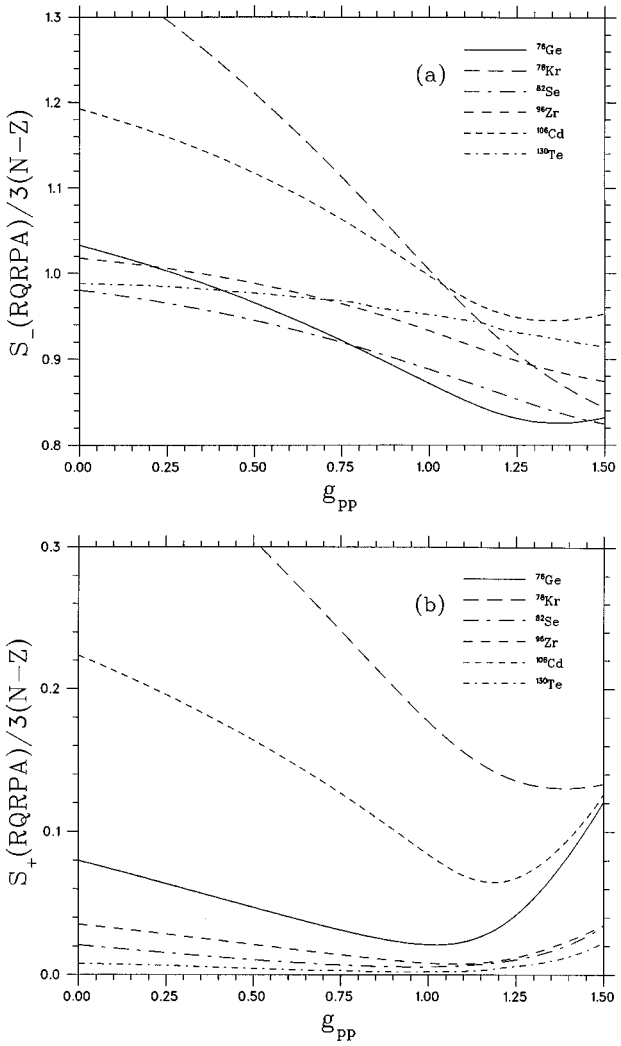

FIG. 7. The same as Fig. 6 in the RQRPA approach. Here the curves have been plotted up to $g_{pp}=1.50$.

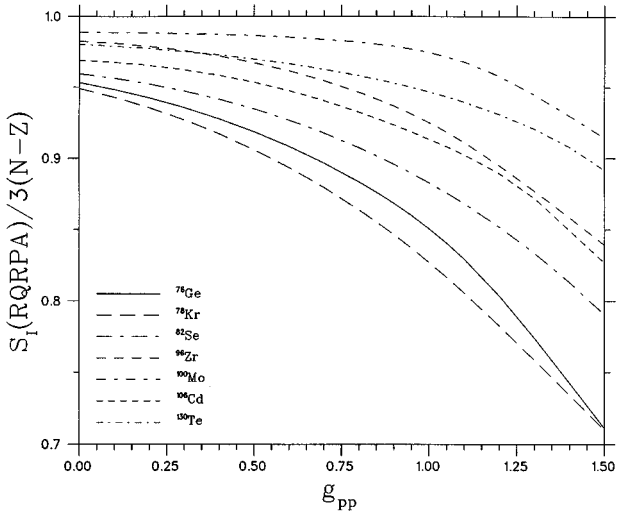

FIG. 8. The ratio of the RQRPA sum $S_I=S_- - S_+$ and the exact sum $3(N-Z)$ as a function of g_{pp} for different $2\nu\beta\beta$ mother nuclei.

sum S_- in the RQRPA for all the other nuclei than ^{76}Ge. For ^{76}Ge both the S_- and the S_+ branches conspire to deteriorate the sum rule. A violation of the sum rule was also found for Fermi-type transitions in the RQRPA using a very schematic model [24]. In [24] the violation was quite small at the point where the pn QRPA collapsed. For very large interaction strengths the violation was found to be almost 50% of the sum rule, exceeding the amount of violation found in the present calculation.

It has to be noted that in realistic RQRPA calculations it is relevant only to investigate the nuclear matrix elements in the very vicinity of $g_{pp}=1.0$ where the deviation from the Ikeda sum rule is small for the heavy nuclei. Thus, at least for these nuclei the RQRPA-predicted $2\nu\beta\beta$ half-lives should be reliable. For bigger deviations from the sum rule, say more than 10%, the RQRPA results begin to lose their accuracy since it is hard to quantify the effects of the sum-rule violation upon the value of the DGT matrix element (see the discussion in [24]).

Next we briefly discuss the differences between the QRPA and the RQRPA in the light of the double-β sum rule of Refs. [25,26]. As pointed out in these articles the double-β sum rule contains a model-independent part and a model-dependent part. The sum rules are different for the 0^+ and 2^+ final states [26] and here we only concentrate on the 0^+ sum rule which was discussed in the context of the QRPA in Ref. [25]. As pointed out in [25], the double Gamow-Teller operator, when applied to the initial ground state $0^+_{\rm g.s}$, leads to two-phonon states of the final nucleus in the RPA framework. These can be coupled to the $J_f=0$ or $J_f=2$ final angular momentum.

The double-β sum rules can be written as [25,26]

$$S^{J=0}_{\rm DGT}\equiv S^{(-)J=0}_{\rm DGT}-S^{(+)J=0}_{\rm DGT}=\langle 0|[\hat{\beta}^+\hat{\beta}^+,\hat{\beta}^-\hat{\beta}^-]|0\rangle$$

$$=6(N-Z)(N-Z+1)+4(N-Z)S_+-R, \quad (13a)$$

$$S^{J=2}_{\rm DGT}\equiv S^{(-)J=2}_{\rm DGT}-S^{(+)J=2}_{\rm DGT}$$

$$=\langle 0|\sum_{\mu=-2}^{2}(-1)^{\mu}[[\hat{\beta}^+\hat{\beta}^+]_{2\mu},[\hat{\beta}^-\hat{\beta}^-]_{2,-\mu}]|0\rangle$$

$$=10(N-Z)(N-Z-2)+\tfrac{20}{3}(N-Z)S_+ +\tfrac{5}{2}R, \quad (13b)$$

where the first terms on the right-hand side are the model-independent part of the sum rule and the second terms can be obtained from the summed Gamow-Teller β^+ strength. The residual term R has a rather complicated structure (see [26]) and its magnitude can be estimated by calculating the left-hand side of Eqs. (13) in the adopted model. Here we evaluate $S^{J=0}_{\rm DGT}$ and the S_+ term in Eq. (13a) by the QRPA and the RQRPA methods to further study the sum-rule nonconservation in the RQRPA formalism.

In Fig. 9 we discuss the behavior of the various components of the double-β sum rule (13a) as a function of g_{pp} for the ^{76}Ge decay. The emerging pattern for the other cases is qualitatively the same. As seen in Fig. 9, the sum of the first two terms on the right-hand side of Eq. (13a) is almost the same for the QRPA and the RQRPA. This is due to the fact that the sum S_+ results almost the same in both models as already discussed in the context of Figs. 6(b) and 7(b).

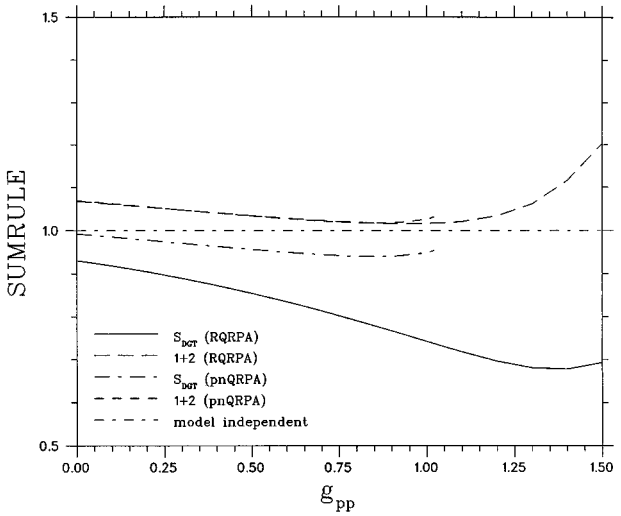

FIG. 9. Various terms of the double-β sum rule of Eq. (13a) as a function of g_{pp} for the ^{76}Ge decay. The model-independent part is depicted by the short dot-dashed line and the sum of the two terms of the model-dependent part by the short dashed line for the QRPA and by the long dashed line for the RQRPA. The total sum rule $S_{\rm DGT}^{J=0}$ has been drawn by a long dot-dashed line (continuous line) for the QRPA (RQRPA). All the curves have been normalized by the factor $6(N-Z)(N-Z+1)$.

Within the QRPA, which satisfies the sum rule exactly, the magnitude of the residual term R tends to be almost independent of g_{pp} and less than 10% of the total sum rule (typically some 5%). For the RQRPA this is not the case due to its inherent violation of the double-β sum rule. As seen in the figure, this violation increases with increasing g_{pp} and is more severe than in the case of the Ikeda sum rule. In both models, as expected, the $S_{\rm DGT}^{(+)J=0}$ contribution to the sum rule is very small in the decays studied, typically less than 1 per mil of the $S_{\rm DGT}^{(-)J=0}$ contribution.

As a final step in our DGT analysis we should like to study what fraction of the double-β sum rules of Eqs. (13) are exhausted by the transitions to the final states $0^+_{\rm g.s.}$, 2^+_1, 0^+_2, and 2^+_2 in the pn QRPA and the RQRPA frameworks. To achieve this we define the ratio

$$\chi(J_f^+)=M_{\rm DGT}^{(c)}(J_f^+)/{\rm DGTSR}(J_f^+), \tag{14}$$

where ${\rm DGTSR}(J_f^+)$ denotes the model-independent part of the sum rules $S_{\rm DGT}^{J=0}$ and $S_{\rm DGT}^{J=2}$ in Eqs. (13) and $M_{\rm DGT}^{(c)}(J_f^+)$ is the closure approximation of the matrix element (9), i.e.,

$$M_{\rm DGT}^{(c)}(J_f^+)=\sum_m \beta_m^+(J_f^+)\beta_m^- . \tag{15}$$

The fraction $\chi(J_f^+)$ has been studied in Table VI for three representative decays in the WS basis (this is the basis which most of the other authors in the field use) for g_{pp} values indicated in Tables IV and V. Both the pn QRPA and the RQRPA results are shown. From this table one can see that the pn QRPA and the RQRPA give very different fractions for the ground-state transition in ^{76}Ge and ^{82}Se and for transitions to the 2^+ final states in the case of ^{76}Ge. Otherwise the two approaches give essentially the same results, especially for the 0^+_2 transitions.

Analysis of the different intermediate contributions to the closure matrix element reveals the reason for the big differences between the two approaches in the case of the ground-state transitions. The closure matrix element contains large negative and sizable positive contributions coming from virtual transitions to high intermediate energies. In the DGT matrix elements these contributions are suppressed by the increasing energy denominator. In the closure approximation the cancellation between the positive and negative contributions is different in the two approaches and thus leads to quite different final values for the two closure matrix elements. Going beyond the closure approximation yields to cancellation which is modulated by the energy denominator leading to a common value for the DGT matrix elements. The excited-state transitions behave differently mainly due to a coherent summation of the intermediate contributions thus avoiding the delicate cancellation effects present in the ground-state transitions.

A general conclusion results from Table VI: the double-β transitions represent a very tiny portion of the double-β sum rule and thus the evaluation of the double-β half-lives relies on the ability of the theory to describe the low-energy tail of the bulk DGT strength. Interestingly enough, the decays to the 0^+_2 state seem to exhaust more of the total DGT strength than the other final states under discussion. The variations of the fraction from nucleus to nucleus seem to be the largest in the case of the ground-state transition due to the above discussed cancellation effects.

IV. CONCLUSIONS

Double-β-decay transition amplitudes and half-lives have been calculated for several nuclei using renormalized pn QRPA, RQRPA for short. The RQRPA yields more realistic

TABLE VI. Fractions $\chi(J_f^+)$ of the double-β sum rule for the final states $J_f^+=0^+_{\rm g.s.},2^+_1,0^+_2,2^+_2$. For the exact definition of $\chi(J_f^+)$ see Eq. (14). The decays of ^{76}Ge, ^{82}Se, and ^{130}Te are taken as representative cases and the g_{pp} values of Tables IV and V are used for the WS basis. For ^{82}Se and ^{130}Te the experimental $\chi(0^+_{\rm g.s.})$ values, extracted in Ref. [24], are 5×10^{-4} and 2×10^{-5}, respectively.

	$\chi(0^+_{\rm g.s.})$		$\chi(2^+_1)$		$\chi(0^+_2)$		$\chi(2^+_2)$	
Nucleus	pn QRPA	RQRPA	pn QRPA	RQRPA	pn QRPA	RQRPA	pn QRPA	RQRPA
^{76}Ge	6.8×10^{-4}	3.2×10^{-3}	8.4×10^{-5}	4.3×10^{-6}	5.0×10^{-3}	4.3×10^{-3}	3.1×10^{-4}	4.8×10^{-5}
^{82}Se	1.3×10^{-3}	3.6×10^{-5}	1.7×10^{-4}	7.3×10^{-5}	2.4×10^{-3}	2.1×10^{-3}	2.8×10^{-4}	2.4×10^{-4}
^{130}Te	8.4×10^{-5}	1.1×10^{-4}	1.7×10^{-5}	1.6×10^{-5}	1.1×10^{-3}	1.0×10^{-3}	3.4×10^{-5}	3.3×10^{-5}

nuclear matrix elements in the physical range ($g_{pp}=0.9-1.1$) of the particle-particle interaction strength than the ordinary pn QRPA. Examples are ^{76}Ge and ^{82}Se, for whom the ground-state half-life has been measured. Furthermore, in comparison with the pn QRPA, the RQRPA gives results which are more independent of the details of the single-particle spectrum.

We have shown that the RQRPA violates the Ikeda sum rule and the double-β sum rule, and that the amount of violation is mass dependent. The amount of violation is small for heavy nuclei and implies reliability of the RQRPA results in these cases. For larger violations one can not access the quality of the RQRPA results and they should be compared to some extended RQRPA approaches in the future.

[1] T. Tomoda, Rep. Prog. Phys. **54**, 53 (1991); M. K. Moe and P. Vogel, Annu. Rev. Nucl. Part. Sci. **44**, 247 (1994).

[2] P. Vogel and M. R. Zirnbauer, Phys. Rev. Lett. **57**, 3148 (1986); J. Engel, P. Vogel, and M. R. Zirnbauer, Phys. Rev. C **37**, 731 (1988).

[3] K. Muto, E. Bender, and H. V. Klapdor-Kleingrothaus, Z. Phys. A **339**, 435 (1991).

[4] D. B. Stout and T. T. S. Kuo, Phys. Rev. Lett. **69**, 1900 (1992); S. S. Hsiao, Y. Tzeng, and T. T. S. Kuo, Phys. Rev. C **49**, 2233 (1994).

[5] O. Civitarese, A. Faessler, J. Suhonen, and X. R. Wu, J. Phys. G **17**, 943 (1991); F. Krmpotić, A. Mariano, T. T. S. Kuo, and K. Nakayama, Phys. Lett. B **319**, 393 (1993).

[6] F. Krmpotić and S. S. Sharma, Nucl. Phys. **A572**, 329 (1994).

[7] A. A. Raduta, A. Faessler, and S. Stoica, Nucl. Phys. **A534**, 149 (1991).

[8] J. Toivanen and J. Suhonen, Phys. Rev. Lett. **75**, 410 (1995).

[9] J. Suhonen, Nucl. Phys. **A563**, 205 (1993); J. Suhonen and O. Civitarese, Phys. Lett. B **308**, 212 (1993).

[10] D. J. Rowe, Rev. Mod. Phys. **40**, 153 (1968).

[11] K. Ikeda, T. Udagawa, and H. Yamaura, Prog. Theor. Phys. **33**, 22 (1965).

[12] D. Karadjov, V. V. Voronov, and F. Catara, Phys. Lett. B **306**, 197 (1993).

[13] F. Catara, N. Dinh Dang, and M. Sambataro, Nucl. Phys. **A579**, 1 (1994).

[14] D. J. Rowe, Phys. Rev. **175**, 1283 (1968).

[15] H. Lenske and J. Wambach, Phys. Lett. B **249**, 377 (1990).

[16] A. Klein, R. Walet, and G. Do Dang, Nucl. Phys. **A535**, 1 (1991).

[17] O. Civitarese and J. Suhonen, Nucl. Phys. **A575**, 251 (1994).

[18] M. Aunola and J. Suhonen, Nucl. Phys. **A602**, 133 (1996).

[19] P. Ring and P. Schuck, *The Nuclear Many-Body Problem* (Springer, New York, 1980).

[20] D. J. Rowe, *Nuclear Collective Motion* (Methuen, London, 1970).

[21] J. Suhonen and O. Civitarese, Phys. Rev. C **49**, 3055 (1994).

[22] A. Raduta and J. Suhonen, Phys. Rev. C **53**, 176 (1996).

[23] F. Alasia and O. Civitarese, Phys. Rev. C **42**, 1335 (1990).

[24] J. G. Hirsch, P. O. Hess, and O. Civitarese, Phys. Rev. C. **54**, 1976 (1996).

[25] P. Vogel, M. Ericson, and J. D. Vergados, Phys. Lett. B **212**, 259 (1988).

[26] K. Muto, Phys. Lett. B **277**, 13 (1992).